Structure and function of broadly reactive antibody PG16 reveal an H3 subdomain that mediates potent neutralization of HIV-1

Robert Pejchal[a], Laura M. Walker[b], Robyn L. Stanfield[a], Sanjay K. Phogat[c], Wayne C. Koff[c], Pascal Poignard[b,d], Dennis R. Burton[b,d,e,1], and Ian A. Wilson[a,d,f,1]

Departments of [a]Molecular Biology and [b]Immunology and Microbial Science, [d]International AIDS Vaccine Initiative Neutralizing Antibody Center, and [f]The Skaggs Institute for Chemical Biology, The Scripps Research Institute, La Jolla, CA 92037; [c]International AIDS Vaccine Initiative, New York, NY 10038; and [e]Ragon Institute of Massachusetts General Hospital, Massachusetts Institute of Technology, and Harvard University, Boston, MA 02114

Edited by David Baker, University of Washington, Seattle, WA, and approved May 7, 2010 (received for review April 6, 2010)

Development of an effective vaccine against HIV-1 will likely require elicitation of broad and potent neutralizing antibodies against the trimeric surface envelope glycoprotein (Env). Monoclonal antibodies (mAbs) PG9 and PG16 neutralize ~80% of HIV-1 isolates across all clades with extraordinary potency and target novel epitopes preferentially expressed on Env trimers. As these neutralization properties are ideal for a vaccine-elicited antibody response to HIV-1, their structural basis was investigated. The crystal structure of the antigen-binding fragment (Fab) of PG16 at 2.5 Å resolution revealed its unusually long, 28-residue, complementarity determining region (CDR) H3 forms a unique, stable subdomain that towers above the antibody surface. A 7-residue "specificity loop" on the "hammerhead" subdomain was identified that, when transplanted from PG16 to PG9 and vice versa, accounted for differences in the fine specificity and neutralization of these two mAbs. The PG16 electron density maps also revealed that a CDR H3 tyrosine was sulfated, which was confirmed for both PG9 (doubly) and PG16 (singly) by mass spectral analysis. We further showed that tyrosine sulfation plays a role in binding and neutralization. An N-linked glycan modification is observed in the variable light chain, but not required for antigen recognition. Further, the crystal structure of the PG9 light chain at 3.0 Å facilitated homology modeling to support the presence of these unusual features in PG9. Thus, PG9 and PG16 use unique structural features to mediate potent neutralization of HIV-1 that may be of utility in antibody engineering and for high-affinity recognition of a variety of therapeutic targets.

neutralizing antibody | PG9 | sulfotyrosine | gp120 | Env

Despite extensive efforts, an effective HIV-1 vaccine remains an elusive goal. In particular, the elicitation of broadly neutralizing antibody (bNAb) responses targeting the envelope glycoproteins (Env) of HIV-1, gp120 and gp41, remains a major challenge. In humans, gp120 subunit vaccines fail to induce antibodies that neutralize primary HIV-1 isolates and do not afford protection against infection (1–5). A range of other potential vaccine candidates have failed to elicit bNAb responses in animals (6–8). However, a proportion of HIV-1–infected individuals develop broadly neutralizing sera over time (9–15), and potent and broadly cross-reactive monoclonal antibodies (mAbs) have been isolated from a few such individuals (16–21). Passive transfer studies in macaques have shown that these bNAbs can completely protect against viral challenge (22–27), suggesting that sufficient titers of preexisting bNAbs may be effective in preventing infection. Structural studies of such bNAbs reveal atomic details of immune recognition of neutralization determinants, which can be used to guide development of novel immunogens aimed at eliciting a more focused response to the most relevant epitopes (28–36).

PG9 and PG16 are recently discovered neutralizing mAbs that possess the breadth and potency desired of an antibody response generated by vaccination (20). Notably, their potency is about an order of magnitude higher than that of previously described broadly neutralizing mAbs to HIV-1. These two antibodies differ by somatic variation and bind to overlapping, but distinct, gp120 epitopes composed of conserved determinants in V2, V3, the V1/V2 stem, and perhaps elements of the coreceptor binding site (CoRbs) (20). The epitopes are preferentially displayed on Env trimers, as expressed on the surface of virions and transfected cells, but are not found on recombinant monomeric gp120 or soluble trimers for the great majority of HIV-1 isolates. Alanine scanning mutagenesis indicates that PG9 and PG16 are equally sensitive to specific substitutions within V1 and V2, whereas PG16 is much more sensitive to changes in V3 (20). These fine specificity differences likely reflect the ability of the immune system to respond to a constantly evolving viral target.

The V2 and V3 domains are located at the apex of the trimeric spike, as determined by fitting crystal structures of core gp120 in complex with the antigen-binding fragment (Fab) into cryoelectron tomography reconstructions of the native trimer (32), and are thought to mediate gp120 protomer association within the trimer (32, 37). However, no crystal structure of a gp120/gp41 trimer exists to model the epitope. In addition, current gp120 structures do not include V1/V2 and may not faithfully mimic the conformation of full-length gp120 in the context of the native spike. Consequently, the atomic details of the gp120 trimer interface and, hence, the PG9 and PG16 epitope, are not known. Nevertheless, it can be inferred that the PG9 and PG16 epitopes exist only on unliganded spikes, as binding of both antibodies is inhibited by a soluble form of the CD4 receptor (20), which induces major conformational rearrangements in the Env trimer, including changes in the relative dispositions of the variable loops (32). They do not compete with CD4bs-directed mAbs, such as b12, that induce fewer conformational rearrangements (32). Additionally, PG9 and PG16 neutralization is dependent on specific N-linked glycans on gp120, which are not visible in crystal structures of HIV core gp120. It is not known whether

IMMUNOLOGY

Author contributions: R.P., L.M.W., S.K.P., W.C.K., D.R.B., and I.A.W. designed research; R.P. and L.M.W. performed research; R.P. and L.M.W. contributed new reagents/analytic tools; R.P., L.M.W., R.L.S., P.P., D.R.B., and I.A.W. analyzed data; and R.P., L.M.W., D.R.B., and I.A.W. wrote the paper.

Conflict of interest statement: L.M.W, S.K.P, P.P, and D.R.B. are inventors on a patent describing the human broadly neutralizing antibodies PG9 and PG16 (United States provisional patent application numbers USSN 61/161,010; USSN 61/165,829; and USSN 61/224,739).

This article is a PNAS Direct Submission.

Freely available online through the PNAS open access option.

Data deposition: The atomic coordinates have been deposited in the Protein Data Bank, www.pdb.org [PDB ID codes 3MUG (PG16 Fab) and 3MUH (PG9 LC)].

[1]To whom correspondence may be addressed. E-mail: burton@scripps.edu or wilson@scripps.edu.

This article contains supporting information online at www.pnas.org/lookup/suppl/doi:10.1073/pnas.1004600107/-/DCSupplemental.

these glycans are recognized directly, contribute to the presentation of the protein epitope, or are involved in the conformational integrity of the trimer.

To gain insight into PG9 and PG16 binding and neutralizing activity, we determined crystal structures of the Fab fragment of PG16, and the PG9 light chain, from which a homology model of Fab PG9 was constructed for comparison with PG16. These structures, along with functional characterization of PG9 and PG16 variants, show that both antibodies are sulfated and use a unique complementarity determining region (CDR) H3 subdomain structure to confer fine specificity and effect potent neutralization of HIV-1.

Results

Structure of Fab PG16. The monoclinic crystals of PG16 Fab (*SI Text* and Table S1) contain six Fab molecules in the asymmetric unit (asu) with three chemically distinct environments: Fab1 [chains A (light) and B (heavy)] and Fab2 (C and D) have similar elbow angles 216° and 221°, respectively, whereas Fab3 (E and F) has a 249° angle. The remaining three Fabs (Fab4, G and H; Fab5, I and J; and Fab6, K and L) are pseudotranslated copies of Fabs1–3 with identical elbow angles to their counterparts. The variation in elbow angles implies flexibility of the PG16 Fab, as noted particularly for antibodies with a λ light chain (38). Fab4 has the lowest overall *B* value and is used here to describe the PG16 structure.

PG16 has a 28-residue CDR H3 (Kabat numbering, Fig. 1), which equals the longest in human antibody sequences to date. The CDR H3 base has a canonical, β-bulge torso conformation (39), which is supported by several contacts between V_L and V_H (Fig. 1). Two such contacts are mediated by L3: Arg^{L96} interacts with Glu^{H95} at the H3 base, and Arg^{L94} forms a salt bridge with Asp^{H61}. Glu^{H95} also hydrogen bonds with framework His^{H35} and the backbone amide of His^{H100R}, further stabilizing a bulge formed by Tyr^{H100Q}-His^{H100R}-Tyr^{H100S} at the end of H3. A stacking interaction is formed between Phe^{L49} and Tyr^{H100S}.

Out of this stable base rises the β-sheet "stalk" of the H3 subdomain structure. The initial ascent is composed of Ala^{H96}-Gly^{H97}-Gly^{H98}, where the Gly residues form an antiparallel β-sheet with Tyr^{H100O} and Asn^{H100P}. The β-sheet is extended by an additional interaction between the Tyr^{H100Q} amide and the Ala^{H96} carbonyl, for a total of three, classical, β-sheet hydrogen bonds. The Gly^{H97}-Gly^{H98} main chain is sandwiched between the aromatic rings of Tyr^{H100Q} and Tyr^{H100N}. The polypeptide then takes a sharp turn at Pro^{H99} that is stabilized by a hydrogen bond between the Pro^{H99} carbonyl and the Tyr^{H100Q} hydroxyl.

The major difference between PG9 and PG16 is a set of seven sequential residues (H100–H100F) toward the N-terminal end of CDR H3 (Fig. 1) that are located in an antiparallel β-sheet that forms loop 1 of the H3 "hammerhead" (Fig. 1); the β-sheet starts at Ile^{H100}, which hydrogen bonds with Tyr^{H100G} and ends with His^{H100B}, which hydrogen bonds with Val^{H100E}. The β-sheet briefly terminates when it crosses over the stalk at Tyr^{H100H}, but resumes with a classical β-sheet interaction between Asp^{H100I} and Gly^{H100M}. A 3_{10}-helical turn (Asp^{H100I}-Asp^{H100L}) then forms loop 2, which is stabilized by a contact between CDR H2 Lys^{H57} and the Asp^{H100L} main chain.

The hammerhead is not significantly influenced by lattice interactions; all three chemically unique environments of H3 show different packing arrangements yet the H3 conformations are in close agreement (*SI Text* and Fig. S1). This implied rigidity is likely due to the 13 stabilizing hydrogen bonds within H3, 11 of which are mediated by the main chain and 2 between the side chain and the main chain (Fig. 1). Furthermore, all H3 residues are in favored (88%) or allowed (12%) regions of the Ramachandran plot. Thus, the observed hammerhead structure is expected to be relatively stable (*SI Text* and Fig. S1).

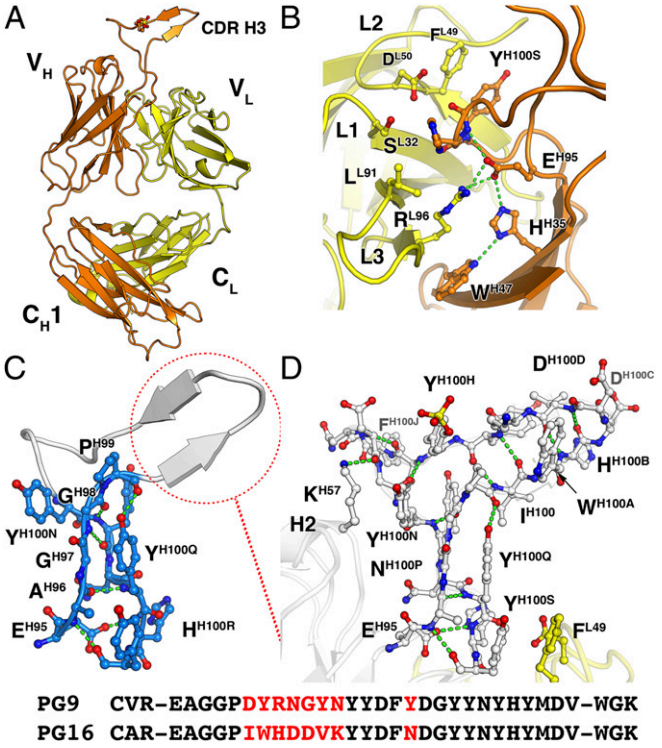

Fig. 1. Overall structure of PG16 Fab illustrating the protrusion of CDR H3 from the combining site. (*A*) Schematic of the PG16 Fab structure with the heavy and light chains shown in orange and yellow ribbon representations, respectively. (*B*) Expanded view of H3 base. Heavy chain (orange) interactions with light chain (yellow) at the base of H3 are depicted. A prominent bulge at the H3 base is stabilized by interactions between Glu^{H95} and the backbone amide of His^{H100R} and supported by interactions of Glu^{H95} with Arg^{L96} and His^{H35} and by stacking of Tyr^{H100Q} with Phe^{L49}. (*C*) Expanded view of H3 stalk region (marine blue). Protrusion of CDR H3 from the variable domain interface is mediated by Gly^{H97}-Gly^{H98}, which are sandwiched between Tyr^{H100N} and Tyr^{H100Q} to form a stalk. The polypeptide takes a sharp turn at Pro^{H99} immediately followed by the variable region loop, which forms a short antiparallel β-sheet. (*D*) Full view of H3. The apex of H3 is composed of Lys^{H100F}, Tyr^{H100G}, Tyr^{H100H}, and Asp^{H100I} that display distorted β-strand geometry as they cross over the stalk region. Tyr^{H100H} is sulfated and the sulfate moiety is ordered (Fig. S3). Asp^{H100I}, Phe^{H100J}, Asn^{H100K}, and Asp^{H100L} form a 3_{10}-helical turn. (*Bottom*) Alignment of the CDR H3 sequences of PG9 and PG16. The seven sequential variable residues that form the short β-sheet "specificity loop" (dashed red circle) are shown in red, as is the only other CDR H3 residue (H100K) that differs between PG9 and PG16.

PG9 Homology Model. The PG9 light chain structure (*SI Text* and Table S2) was used to construct a homology model using the PG16 Fv as a template (*SI Text* and Fig. S2). Comparison of the PG16 structure with the PG9 model reveals that the V_L/V_H contacts visualized in PG16 are reproduced (Fig. S2). The largest differences are in seen in L3; however, the two salt bridges between L3 and V_H in PG16 are also conserved in PG9. Moreover, the stalk structure is likely to be highly similar in PG9 because all important residues are conserved.

Glycosylation of the Light Chains of PG9 and PG16. The PG9 and PG16 light chains contain a predicted glycosylation site at Asn^{L24}. Glycosylation was confirmed in the PG16 Fab and PG9 light chain structures, where the two N-acetylglucosamine moieties attached to Asn^{L24} are ordered in the electron density maps (Fig. S3).

We investigated the role of this glycan modification in Env recognition by testing the effect of deglycosylation of PG9 and PG16 on neutralization of JR-CSF and YU2 pseudoviruses. Neutralization of YU2 by Endo F-treated PG9 and PG16 was

indistinguishable from fully glycosylated forms (Fig. 2), whereas neutralization of JR-CSF was modestly improved. Thus, glycosylation of PG9 and PG16 light chains appears to have a negligible effect on neutralization.

Tyrosine Sulfation in PG9 and PG16. The crystal structure of PG16 Fab revealed a sulfotyrosine modification of Tyr^{H100H} (Fig. 1 and Fig. S3). As sulfation was unexpected, electrospray mass spectrometry (ESI-MS) was used to unequivocally establish its presence in PG9 and PG16. Recombinant Fab from HEK 293S GnTI −/− cells (*Materials and Methods*) is amenable to ESI-MS analysis, as this cell line confers homogenous $Man_5GlcNac_2$ N-glycosylation. ESI-MS identified two sulfoforms of glycosylated PG9: doubly (PG9-S2) and singly sulfated (PG9-S1) (Table 1). Two species of PG16 were also identified: a singly sulfated form (PG16-S1), used to obtain diffracting crystals, and a nonsulfated form (PG16-NS). A PG16 glycan knockout variant, Asn^{L24}→Thr, verified that sulfate was present in the absence of glycan modification and confirmed that the major expressed form is singly sulfated. Anti-sulfotyrosine mAb Sulfo-1C-A2 (Millipore) was used to further validate that the modifications conferring increased mass are sulfotyrosine (*SI Text* and Fig. S4).

As the heterogeneity in sulfation was surprising, we next determined whether tyrosine sulfation is functionally important. Hypersulfation of glycosylated PG9 Fab enhanced, but was not required for, neutralization (Fig. 2); a Mono S fraction enriched in PG9-S2 gave an ∼10-fold decrease in IC_{50} compared with a sample containing only PG9-S1. Sulfated PG16 also showed increased neutralization potency over its nonsulfated form (Fig. 2). Moreover, the Tyr^{H100H} → Phe variant, expected to disrupt sulfation, showed a 2.2-fold increase in IC_{50} (Table 2).

We next examined the effect of mutating sites on Env known to interact with the sulfated N terminus of the HIV-1 chemokine receptor CCR5, as well as sulfotyrosines on CD4-induced (CD4i) antibodies. One sulfotyrosine in the Fab 412d-gp120 structure interacts with residues at the base of V3 of gp120, including Arg298, Asn300, Asn302, Ile322, and Ile326 (40). Of these, only Asn302 → Ala was previously investigated, whereas the Arg298 → Ala variant is noninfectious (20). However, as Asn302 → Ala had no effect on neutralization by PG9 and PG16, we focused on the second interaction site (Arg327, Gln422, and Arg419) that is closer to the bridging sheet. Although Arg419 → Ala had a modest effect on neutralization, increasing the IC_{50} by 3-fold for both PG9 and PG16, Gln422 → Ala showed a 9- and a 5-fold increase in IC_{50} for PG9 and PG16, respectively. Accordingly, we tested the Arg327 → Ala variant and observed an ∼10-fold increase in IC_{50} (Fig. 2), consistent with possible interaction of sulfotyrosine with the coreceptor binding site.

Mutagenesis of PG9 and PG16. On the basis of the crystal structure of PG16, we reasoned that the unusual hammerhead architecture of the CDR H3 subdomain might play a significant role in Env binding and neutralization. Therefore, we focused on this region for functional studies. Because the CDR H3s of PG9 and PG16 differ by seven sequential residues that compose loop 1 (PG9, Asp^{H100}, Tyr^{H100A}, Arg^{H100B}, Asn^{H100C}, Gly^{H100D}, Tyr^{H100E}, and Asn^{H100F}; PG16, Ile^{H100}, Trp^{H100A}, His^{H100B}, Asp^{H100C}, Asp^{H100D}, Val^{H100E}, and Lys^{H100F}), it seemed plausible that this region was responsible for the differences in fine specificity. Thus, we exchanged this seven-residue stretch between antibodies and tested the resulting PG9 and PG16 "swap" variants in functional assays. As PG16 is considerably more potent than PG9 against HIV-1 isolates ADA and YU2, we first tested the PG16 swap variants for neutralizing activity (Fig. 3). Indeed, the PG16 swap variant exhibited a neutralization profile that faithfully mimicked that of PG9. Another important difference is that PG16 exhibits exclusive specificity for membrane-embedded, trimeric HIV-1 Env, whereas PG9 binds to monomeric gp120 from certain isolates, such as DU422, with moderate affinity. Therefore, we tested binding of the PG9 and PG16 swap variants to monomeric gp120 from DU422 (Fig. 3). The PG16 swap variant bound with similar affinity to wild-type PG9, whereas the PG9 swap variant failed to bind, again mapping differences in specificity to this seven-residue stretch in CDR H3.

We then investigated the contribution of individual residues within the seven-residue "specificity loop." PG9 and PG16 variants containing single alanine substitutions were tested for binding activity against DU422 gp120 and neutralizing activity against JR-CSF (Table 2). Neutralization by PG9 was not significantly reduced by substitution of any single residue; however, Asp^{H100} → Ala showed >50-fold reduction in half-maximal binding to DU422 gp120. In addition to any direct interactions with gp120, substitution of Asp^{H100}, one of only three aspartates in PG9 H3, may also compromise sulfation, contributing further to loss in binding. For PG16, hydrophobic residues, Ile^{H100} and Trp^{H100A}, were identified to be important for neutralization, with the latter showing >50-fold increase in IC_{50}.

We then evaluated a panel of variants to assess the contribution of specific residues composing the distorted β-strand atop the H3 subdomain (Val^{H100E}-Asn^{H100K} for PG16 and Tyr^{H100E}-Tyr^{H100K} for

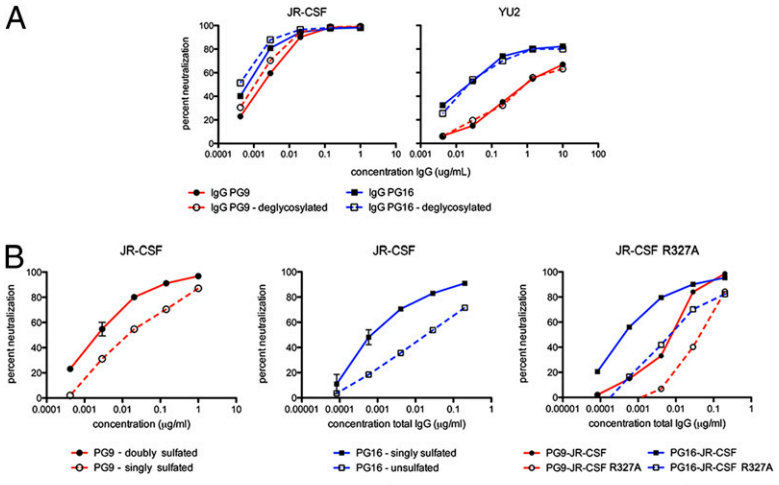

Fig. 2. Role of posttranslational modifications in neutralization of HIV-1 by PG9 and PG16. (*A*) Effect of enzymatic deglycosylation of PG9 and PG16 IgGs on neutralization of JR-CSF and YU2 pseudovirus. Curves shown are for control PG9 IgG (solid black circles, solid red line) and PG16 IgG (solid black squares, solid blue line) and deglycosylated PG9 IgG (open black circles, dashed red line) and PG16 IgG (open black squares, dashed blue line). Endo F treatment of PG9 and PG16 slightly increased neutralization potency against JR-CSF, but had no effect on neutralization of YU2. (*B*) Effect of tyrosine sulfation on neutralization of JR-CSF. Neutralization mediated by a sample of PG9 Fab enriched in the hypersulfated (PG9-S2) form (solid black circles, solid red line) was compared with a pool containing only the hyposulfated form (PG9-S) (open black circles, dashed red line). Neutralization mediated by sulfated PG16 Fab (solid black squares, solid blue line) was compared with nonsulfated PG16 Fab (open black squares, dashed blue line). For both PG9 and PG16, the more sulfated species is the more potent. Neutralization of WT JR-CSF by PG9 (solid black circles, solid red line) and PG16 IgG (solid black squares, solid blue line) was compared with neutralization of JR-CSF containing an R327A substitution by PG9 (open black circles, dashed red line) and PG16 (open black squares, dashed blue line).

Table 1. Electrospray (ESI-MS) mass spectral analysis of purified WT and mutant PG9 and PG16 Fabs

PG9/16 Fab species	Expected mass, Da	ESI-MS mass, Da	Δ mass, species 1 vs. 2	Sulfotyrosines
$Man_5GlcNac_2$ PG9-S2	50,267	50,270	+80	2
$Man_5GlcNac_2$ PG9-S1	50,188	50,190	−80	1
$Man_5GlcNac_2$ PG16-S1	50,125	50,127	+79	1
$Man_5GlcNac_2$ PG16-NS	50,046	50,048	−79	0
Asn^{L24}Thr PG16-S1	48,895	48,897	+80	1
Asn^{L24}Thr PG16-NS	48,816	48,817	−80	0

Expected masses were calculated using averaged isotopic masses and assuming N-terminal pyroglutamic acid conversion of both light and heavy chains, the attachment of a single $Man_5GlcNac_2$ N-linked glycan, as expected for production in HEK 293S GnTI −/− cells, and sulfation.

PG9), which are mostly preserved from the germ-line sequence. For both PG9 and PG16, Asp^{H100I} → Ala showed greatly diminished binding and neutralizing activity, indicating that it makes an important contribution to Env recognition. For PG9, Tyr^{H100H} → Ala also showed reduced neutralization potency compared with WT. Interestingly, Tyr^{H100E} → Ala and Phe^{H100J} → Ala variants neutralized with comparable potency as WT PG9, but bound to gp120 with reduced affinity. However, a good overall correlation was observed for neutralization of JR-CSF and binding to DU422 gp120 monomer by PG9.

On the basis of the PG16 structure, the aromatic rings of Tyr^{H100Q} and Tyr^{H100N} appear to stabilize the stalk of the H3 subdomain. To gain insight into whether this aromatic glycine sandwich is required for Env recognition, we mutated these residues individually to alanine and tested the mutants for neutralizing activity against JR-CSF. Indeed, PG16 Tyr^{H100N} → Ala and Tyr^{H100Q} → Ala showed 11-fold and 40-fold reduced neutralization efficacy, respectively, compared with WT PG16. Similarly, PG9 Tyr^{H100N} → Ala and Tyr^{H100Q} → Ala showed 9- and 12-fold reduced neutralization efficacy compared with WT PG9, respectively.

Discussion

The crystal structure of PG16 reveals that this broad and potent HIV-1 Env trimer-specific antibody possesses a unique hammerhead H3 subdomain structure that is composed of unusual features compared with any other known antibodies: a stable stalk mediating extensive H3 protrusion from the combining site and two interconnected loops, one of which varies between PG9 and PG16 and appears to confer fine specificity. The structure and mass spectrometry data reveal that PG16 is sulfated at Tyr^{H100H}. PG9 is also sulfated and, moreover, found in a hypersulfated form with two sulfate modifications. Functional studies reveal that sulfation contributes to neutralization and may play a role in the observed specificity differences between PG9 and PG16. These data further suggest that PG9 and PG16 may be able to access sulfotyrosine interaction sites within the coreceptor binding site.

The combined JR-CSF neutralization and DU422 binding data indicate that the Tyr^{H100G}-Tyr^{H100H}-Asp^{H100I}-Phe^{H100J} sequence, encoded by the IGHD3-3*01 diversity gene and conserved between PG9 and PG16, is crucial for binding and neutralization of HIV-1. Indeed, Asp^{H100I} is the most critical residue for both PG9

Table 2. Effect of amino acid substitutions in PG9 and PG16 on neutralization of isolate JR-CSF and binding to DU422 gp120

CDR	Substitution	PG9 fold increase in IC50 relative to WT (JR-CSF)	PG9 fold increase in DU422 gp120 half-maximal binding	CDR	Substitution	PG16 fold increase in IC50 relative to WT (JR-CSF)
H1	S30-R31-Q32/ H30-K31-Y32	1		H1	H30-K31-Y32/ S30-R31-Q32	2
H2	Y52 → D	12	10	H2	D52 → Y	1
H3	P99 → A	10	1	H3	P99 → A	2.4
H3	D100 → A	2	>50	H3	I100 → A	12
H3	Y100A → A	2	1.5	H3	W100A → A	>50
H3	R100B → A	0.6	2	H3	H100B → A	2
H3	G100D → A	2	5	H3	D100D → A	4
H3	Y100E → F	4	1			
H3	Y100E → A	1.5	8	H3	V100E → A	0.47
H3	N100F → A	0.65	1	H3	K100F → A	0.08
H3	Y100G → A	16	>30	H3	Y100G → A	4
H3	Y100H → F	22	10	H3	Y100H → F	2.2
H3	D100I → A	>400	>30	H3	D100I → A	200
H3	F100J → A	2	>10	H3	F100J → A	0.5
H3	Y100K → A	1.9	5	H3	N100K → A	0.6
H3	Y100N → F	5	2	H3	Y100N → F	1
H3	Y100N → A	9	10	H3	Y100N → A	11
H3	Y100Q → A	12	10	H3	Y100Q → A	44
H3	PG16-9H3N	0.9		H3	PG9-16H3N	0.68
H3	PG16-9H3Y	1		H3	PG9-16H3Y	0.55
H3	PG9-G7	>500		H3	PG16-G7	>500

Fold increase in neutralization IC_{50}. Substitutions are listed using a one-letter amino acid code. H3 swap variants are designated PG16-9H3N, seven-residue exchange; PG16-9H3Y, seven-residue exchange and Asn^{H100K} → Tyr; PG16-G7, seven residues substituted by polyglycine; PG9-16H3Y, seven-residue exchange; PG9-16H3N, seven-residue exchange and Tyr^{H100K} → Asn; and PG9-G7, seven residues substituted by polyglycine (text and Fig. 1).

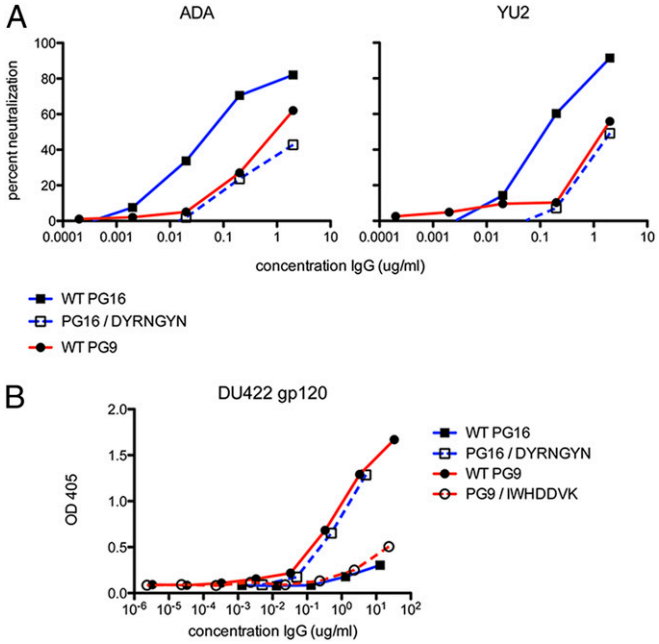

Fig. 3. Neutralization and binding data for the PG9 and PG16 CDR H3-swap variant antibodies. (*A*) Neutralization of PG16-hypersensitive strains ADA and YU2 by WT PG16 IgG (solid black squares, solid blue line), WT PG9 IgG (solid black circles, solid red line), and the PG16/DYRNGYN swap variant (open squares, dashed blue line). Swapping of PG9 H3 variable residues into PG16 confers a neutralization profile that is closely similar to that of PG9. (*B*) Recognition of monomeric DU422 gp120 by WT and H3 swap mutants, determined by ELISA. WT PG9 (solid black circles, solid red line) and the PG16/DYRNGYN swap variant (open squares, dashed blue line) display similar binding profiles with monomeric DU422 gp120. Likewise, PG16 (solid black squares, solid blue line) and the PG9/IWHDDVK swap mutant (open circles, dashed red line) show lack of appreciable binding to DU422 gp120.

and PG16 among the positions that we tested and its substitution by alanine strongly compromises neutralization by both antibodies. Tyr^{H100H}, the only sulfotyrosine in PG16, and, presumably, a site of sulfation in PG9, is also located in this region. However, the same IGHD3-3*01-encoded Tyr^{H100B}-Tyr^{H100C}-Asp^{H100D}-Phe^{H100E} sequence in the 24-residue H3 of nonneutralizing Fab T13 (41) is not sulfated (*SI Text* and Table S3), underscoring the importance of structural context for sulfation.

PG16 is surprisingly tolerant of mutations within CDRs H1 and H2 and is compromised only by substitutions at Trp^{H100A}, Asp^{H100I}, and Tyr^{H100Q} in H3. PG9 is compromised by substitutions at Asp^{H100}, Tyr^{H100G}, Tyr^{H100H}, Asp^{H100I}, and Phe^{H100J} and is generally more sensitive to mutations within H2 and H3. Replacement of the seven variable residues by a polyglycine linker completely abolished neutralization for both antibodies (Table 2). Thus, important contacts to gp120 can be localized largely to the specificity loop and the topmost β-strand of the H3 subdomain.

We asked whether tyrosine sulfation is functionally important by testing the neutralization potency of all of the sulfoforms resolved by Mono S. For both PG9 and PG16, the hypersulfated form neutralized more potently than the hyposulfated (nonsulfated for PG16) species. Heterogeneity of sulfation may be a consequence of the extensive secondary structure found in H3, which may make it a less suitable substrate for tyrosyl protein sulfotransferase. The observation that PG9 is capable of being hypersulfated is reminiscent of known CD4i antibodies: 412d has two sulfotyrosine modifications (40), and E51 has three (42). However, PG9 and PG16 break with established trends set by known CD4i antibodies (43) as they compete with CD4 and are highly dependent on V2 and V3 elements not normally associated with CoRbs binding. Nevertheless, the tyrosines of the extra long H3s of PG9 and PG16 are embedded in an environment enriched in acidic residues, a prerequisite for sulfation (44).

Direct structural information is not available for V1/V2 or for the quaternary interactions at the trimer interface, which likely include V3 and elements of the CoRbs (45). Recent studies suggest that the β20–β21 strands that form part of the bridging sheet in the CD4-liganded state may contribute to stabilization of a conformation of gp120 that promotes better protomer contacts in the unliganded spike (45–47). It has also been suggested that the β20–β21 strands are proximal to V3 and, moreover, may directly interact with a hydrophobic patch containing highly conserved residues near the V3 crown (45). Mutation of these hydrophobic residues (Ile307, Ile309, Phe317, and Tyr318) also strongly knocks down PG16 neutralization (20). Furthermore, residues important for PG9 and PG16 recognition are located within the CoRbs, close to known sites of sulfotyrosine interaction in the bridging sheet and V3 base, as visualized in the structure of antibody 412d with gp120 (40). Thus, it seems plausible that the V2 and V3 elements important for PG9 and PG16 recognition are also located proximal to the gp120 core in the unliganded trimer, where functional requirements for trimerization provide strong selective pressure for conservation. Taken together with observations that CD4 induces large conformational rearrangements in the orientation of gp120 and changes in the location of variable loops in the trimer (32) including exposure of V3, it seems possible that PG9 and PG16 bind closer to the gp120 core, rather than to the very apex of the trimer where the more highly variable residues and glycans are located.

It will be interesting to see whether PG9 and PG16 then represent a unique class of neutralizing antibodies. With the anticipation of new bNAb discoveries (20, 48), it should soon become clear whether elicitation of antibodies against the potent neutralization site recognized by PG9 and PG16 is more common than currently appreciated. A crucial question in this regard is whether the unique architecture of the H3 subdomain, observed in PG16, is a requirement for epitope recognition. Sufficiently long exposure to the proper antigen, such as in chronic infection, may be one factor that pushes the immune system to sample increasingly longer CDR H3s. If a very long H3 is absolutely necessary to elicit antibodies like PG9 and PG16, immunogen design and vaccination strategies may have to take this into consideration. What is exciting and unique is that these very long CDR H3 loops can form subdomains that appear to impart most of the specificity and affinity. Indeed, the specificity loop identified here should be a good template for randomization, which may yield variant PG9 and PG16 with unique specificities. Such findings may have significant ramifications for the design and engineering of human antibodies for therapy, such as for cancer and for infectious diseases.

Materials and Methods

PG9, PG16, and T13 Fabs were produced by cotransfection of plasmids encoding light and heavy chain pairs in HEK 293T or 293S GnTI –/– cells (49). PG9 and PG16 Fabs were purified using an anti-human λ affinity matrix (CaptureSelect Fab λ; BAC), followed by cation exchange. T13 Fab was purified using Protein G Sepharose 4 Fast Flow (GE HealthCare), followed by cation exchange. Fab molecular weights were determined by ESI-MS. PG16 Fab was crystallized by the sitting drop vapor diffusion method and diffraction data were collected on cryoprotected crystals. The structure in $P2_1$ was solved by molecular replacement and refined. Resolved sulfoforms and variant IgG and Fab were tested for neutralization efficacy, using a single round of replication pseudovirus assay and binding by ELISA. Full methods are detailed in *SI Materials and Methods*.

ACKNOWLEDGMENTS. We thank the staff at General Medicine and Cancer Institutes Collaborative Access Team at the Advanced Photon Source and X. Dai for assistance with data collection, D. Marciano and H. Tien of the Joint

Center for Structural Genomics for assistance with the International AIDS Vaccine Initiative/The Scripps Research Institute/Joint Center for Structural Genomics CrystalMation robot, R. Stefanko for technical help, J. Binley (Torrey Pines Institute for Molecular Studies, San Diego) for the gift of E51 IgG, H. Gobind Khorana (Massachusetts Institute of Technology, Cambridge, MA) for the gift of HEK 293S cells, and Peter D. Kwong and Richard Lerner for helpful discussions. Monoclonal antibodies PG9 and PG16 were provided for initial experiments by Theraclone Sciences. This work was supported by National Institutes of Health Grants AI84817 (to I.A.W. and R.L.S.) and AI33292 (to D.R.B.), by National Institutes of Health/National Institute of Allergy and Infectious Diseases National Research Service Award fellowship AI74372 (to R.P.), and by the International AIDS Vaccine Initiative Neutralizing Antibody Center. This is manuscript 20640-MB from The Scripps Research Institute.

1. Mascola JR, et al; The National Institute of Allergy and Infectious Diseases AIDS Vaccine Evaluation Group (1996) Immunization with envelope subunit vaccine products elicits neutralizing antibodies against laboratory-adapted but not primary isolates of human immunodeficiency virus type 1. *J Infect Dis* 173:340–348.
2. Flynn NM, et al.; rgp120 HIV Vaccine Study Group (2005) Placebo-controlled phase 3 trial of a recombinant glycoprotein 120 vaccine to prevent HIV-1 infection. *J Infect Dis* 191:654–665.
3. Gilbert PB, et al. (2005) Correlation between immunologic responses to a recombinant glycoprotein 120 vaccine and incidence of HIV-1 infection in a phase 3 HIV-1 preventive vaccine trial. *J Infect Dis* 191:666–677.
4. Moore JP, et al. (1995) Primary isolates of human immunodeficiency virus type 1 are relatively resistant to neutralization by monoclonal antibodies to gp120, and their neutralization is not predicted by studies with monomeric gp120. *J Virol* 69:101–109.
5. Pitisuttithum P, et al.; Bangkok Vaccine Evaluation Group (2006) Randomized, double-blind, placebo-controlled efficacy trial of a bivalent recombinant glycoprotein 120 HIV-1 vaccine among injection drug users in Bangkok, Thailand. *J Infect Dis* 194: 1661–1671.
6. Phogat S, Wyatt R (2007) Rational modifications of HIV-1 envelope glycoproteins for immunogen design. *Curr Pharm Des* 13:213–227.
7. Montero M, van Houten NE, Wang X, Scott JK (2008) The membrane-proximal external region of the human immunodeficiency virus type 1 envelope: Dominant site of antibody neutralization and target for vaccine design. *Microbiol Mol Biol Rev* 72: 54–84.
8. Scanlan CN, Offer J, Zitzmann N, Dwek RA (2007) Exploiting the defensive sugars of HIV-1 for drug and vaccine design. *Nature* 446:1038–1045.
9. Corti D, et al. (2010) Analysis of memory B cell responses and isolation of novel monoclonal antibodies with neutralizing breadth from HIV-1-infected individuals. *PLoS ONE* 5:e8805.
10. Li Y, et al. (2009) Analysis of neutralization specificities in polyclonal sera derived from human immunodeficiency virus type 1-infected individuals. *J Virol* 83: 1045–1059.
11. Sather DN, et al. (2009) Factors associated with the development of cross-reactive neutralizing antibodies during human immunodeficiency virus type 1 infection. *J Virol* 83:757–769.
12. Binley JM, et al. (2008) Profiling the specificity of neutralizing antibodies in a large panel of plasmas from patients chronically infected with human immunodeficiency virus type 1 subtypes B and C. *J Virol* 82:11651–11668.
13. Gray ES, et al. (2009) Broad neutralization of human immunodeficiency virus type 1 mediated by plasma antibodies against the gp41 membrane proximal external region. *J Virol* 83:11265–11274.
14. Dhillon AK, et al. (2007) Dissecting the neutralizing antibody specificities of broadly neutralizing sera from human immunodeficiency virus type 1-infected donors. *J Virol* 81:6548–6562.
15. Li Y, et al. (2007) Broad HIV-1 neutralization mediated by CD4-binding site antibodies. *Nat Med* 13:1032–1034.
16. Burton DR, et al. (1994) Efficient neutralization of primary isolates of HIV-1 by a recombinant human monoclonal antibody. *Science* 266:1024–1027.
17. Purtscher M, et al. (1994) A broadly neutralizing human monoclonal antibody against gp41 of human immunodeficiency virus type 1. *AIDS Res Hum Retroviruses* 10: 1651–1658.
18. Stiegler G, et al. (2001) A potent cross-clade neutralizing human monoclonal antibody against a novel epitope on gp41 of human immunodeficiency virus type 1. *AIDS Res Hum Retroviruses* 17:1757–1765.
19. Trkola A, et al. (1996) Human monoclonal antibody 2G12 defines a distinctive neutralization epitope on the gp120 glycoprotein of human immunodeficiency virus type 1. *J Virol* 70:1100–1108.
20. Walker LM, et al. (2009) Protocol G Principal Investigators (2009) Broad and potent neutralizing antibodies from an African donor reveal a new HIV-1 vaccine target. *Science* 326:285–289.
21. Zwick MB, et al. (2001) Broadly neutralizing antibodies targeted to the membrane-proximal external region of human immunodeficiency virus type 1 glycoprotein gp41. *J Virol* 75:10892–10905.
22. Mascola JR, et al. (1999) Protection of macaques against pathogenic simian/human immunodeficiency virus 89.6PD by passive transfer of neutralizing antibodies. *J Virol* 73:4009–4018.
23. Mascola JR, et al. (2000) Protection of macaques against vaginal transmission of a pathogenic HIV-1/SIV chimeric virus by passive infusion of neutralizing antibodies. *Nat Med* 6:207–210.
24. Parren PW, et al. (2001) Antibody protects macaques against vaginal challenge with a pathogenic R5 simian/human immunodeficiency virus at serum levels giving complete neutralization in vitro. *J Virol* 75:8340–8347.
25. Shibata R, et al. (1999) Neutralizing antibody directed against the HIV-1 envelope glycoprotein can completely block HIV-1/SIV chimeric virus infections of macaque monkeys. *Nat Med* 5:204–210.
26. Hessell AJ, et al. (2009) Broadly neutralizing human anti-HIV antibody 2G12 is effective in protection against mucosal SHIV challenge even at low serum neutralizing titers. *PLoS Pathog* 5:e1000433.
27. Hessell AJ, et al. (2010) Broadly neutralizing monoclonal antibodies 2F5 and 4E10 directed against the human immunodeficiency virus type 1 gp41 membrane-proximal external region protect against mucosal challenge by simian-human immunodeficiency virus SHIVBa-L. *J Virol* 84:1302–1313.
28. Calarese DA, et al. (2003) Antibody domain exchange is an immunological solution to carbohydrate cluster recognition. *Science* 300:2065–2071.
29. Cardoso RM, et al. (2005) Broadly neutralizing anti-HIV antibody 4E10 recognizes a helical conformation of a highly conserved fusion-associated motif in gp41. *Immunity* 22:163–173.
30. Julien JP, Bryson S, Nieva JL, Pai EF (2008) Structural details of HIV-1 recognition by the broadly neutralizing monoclonal antibody 2F5: Epitope conformation, antigen-recognition loop mobility, and anion-binding site. *J Mol Biol* 384:377–392.
31. Kwong PD, Wilson IA (2009) HIV-1 and influenza antibodies: Seeing antigens in new ways. *Nat Immunol* 10:573–578.
32. Liu J, Bartesaghi A, Borgnia MJ, Sapiro G, Subramaniam S (2008) Molecular architecture of native HIV-1 gp120 trimers. *Nature* 455:109–113.
33. Ofek G, et al. (2004) Structure and mechanistic analysis of the anti-human immunodeficiency virus type 1 antibody 2F5 in complex with its gp41 epitope. *J Virol* 78: 10724–10737.
34. Pejchal R, et al. (2009) A conformational switch in human immunodeficiency virus gp41 revealed by the structures of overlapping epitopes recognized by neutralizing antibodies. *J Virol* 83:8451–8462.
35. Saphire EO, et al. (2001) Crystal structure of a neutralizing human IGG against HIV-1: A template for vaccine design. *Science* 293:1155–1159.
36. Zhou T, et al. (2007) Structural definition of a conserved neutralization epitope on HIV-1 gp120. *Nature* 445:732–737.
37. Schief WR, Ban YE, Stamatatos L (2009) Challenges for structure-based HIV vaccine design. *Curr Opin HIV AIDS* 4:431–440.
38. Stanfield RL, Zemla A, Wilson IA, Rupp B (2006) Antibody elbow angles are influenced by their light chain class. *J Mol Biol* 357:1566–1574.
39. Al-Lazikani B, Lesk AM, Chothia C (1997) Standard conformations for the canonical structures of immunoglobulins. *J Mol Biol* 273:927–948.
40. Huang CC, et al. (2007) Structures of the CCR5 N terminus and of a tyrosine-sulfated antibody with HIV-1 gp120 and CD4. *Science* 317:1930–1934.
41. Walker LM, Bowley DR, Burton DR (2009) Efficient recovery of high-affinity antibodies from a single-chain Fab yeast display library. *J Mol Biol* 389:365–375.
42. Choe H, et al. (2003) Tyrosine sulfation of human antibodies contributes to recognition of the CCR5 binding region of HIV-1 gp120. *Cell* 114:161–170.
43. Huang CC, et al. (2004) Structural basis of tyrosine sulfation and VH-gene usage in antibodies that recognize the HIV type 1 coreceptor-binding site on gp120. *Proc Natl Acad Sci USA* 101:2706–2711.
44. Stone MJ, Chuang S, Hou X, Shoham M, Zhu JZ (2009) Tyrosine sulfation: An increasingly recognised post-translational modification of secreted proteins. *N Biotechnol* 25:299–317.
45. Xiang SH, et al. (2010) A V3 loop-dependent gp120 element disrupted by CD4 binding stabilizes the human immunodeficiency virus (HIV-1) envelope glycoprotein trimer. *J Virol* 84:3147–3161.
46. Finzi A, et al. (2010) Topological layers in the HIV-1 gp120 inner domain regulate gp41 interaction and CD4-triggered conformational transitions. *Mol Cell* 37:656–667.
47. Pancera M, et al. (2010) Structure of HIV-1 gp120 with gp41-interactive region reveals layered envelope architecture and basis of conformational mobility. *Proc Natl Acad Sci USA* 107:1166–1171.
48. Simek MD, et al. (2009) Human immunodeficiency virus type 1 elite neutralizers: Individuals with broad and potent neutralizing activity identified by using a high-throughput neutralization assay together with an analytical selection algorithm. *J Virol* 83:7337–7348.
49. Reeves PJ, Callewaert N, Contreras R, Khorana HG (2002) Structure and function in rhodopsin: High-level expression of rhodopsin with restricted and homogeneous N-glycosylation by a tetracycline-inducible N-acetylglucosaminyltransferase I-negative HEK293S stable mammalian cell line. *Proc Natl Acad Sci USA* 99:13419–13424.